RESEARCH ARTICLE

National Science Open
4: 20250005, 2025
https://doi.org/10.1360/nso/20250005

Materials Science

Special Topic: Thermoelectric Materials and Devices

Robust mechanical properties of $Ag_2Se_{1-x}Te_x$ thermoelectric materials

Heyang Chen[1,#], Shenghong Ren[2,3,#], Hengyang Feng[1], Tian-Ran Wei[1,4,*], Ling Fu[1], Zhenyu Pan[1,*], Kunpeng Zhao[1,4], Xiuyan Li[2] & Xun Shi[1,5,*]

[1] *State Key Laboratory of Metal Matrix Composites, School of Materials Science and Engineering, Shanghai Jiao Tong University, Shanghai 200240, China;*
[2] *Institute of Metal Research, Chinese Academy of Sciences, Shenyang 110016, China;*
[3] *School of Materials Science and Engineering, University of Science and Technology of China, Hefei 230026, China;*
[4] *Wuzhen Laboratory, Tongxiang 314500, China;*
[5] *State Key Laboratory of High Performance Ceramics and Superfine Microstructures, Shanghai Institute of Ceramics, Chinese Academy of Sciences, Shanghai 200050, China*

#Contributed equally to this work.

Received 4 February 2025; Revised 15 April 2025; Accepted 18 April 2025; Published online 30 April 2025

Abstract: High mechanical robustness is essential to the material's processibility for the applications in flexible and miniaturized electronics. As state-of-the-art room-temperature thermoelectric materials, $Ag_2Se_{1-x}Te_x$ alloys exhibit superior thermoelectric transport properties but their mechanical properties remain largely unexplored. Herein, we systematically investigate the mechanical and thermoelectric properties of a series of $Ag_2Se_{1-x}Te_x$ materials. Among them, $Ag_2Se_{0.9}Te_{0.1}$ shows robust mechanical properties including a large compression strain of (26.7 ± 4.5)%, a high compression strength of (279.2 ± 49) MPa, and an excellent fracture toughness of (4.5 ± 0.6) MPa $m^{1/2}$. These robust mechanical properties are ascribed to the dense dislocations as well as possible sub-grain rotations. Combined with the excellent thermoelectric figure of merit, zT of 0.78 at 300 K and 1.1 at 380 K, the $Ag_2Se_{1-x}Te_x$ alloys are promising candidates for robust and efficient thermoelectric applications near room temperature.

Keywords: thermoelectric, Ag_2Se-Ag_2Te, mechanical properties

INTRODUCTION

Thermoelectric materials enable the direct conversion between heat and electricity, providing a promising solution for green energy utilization and environmental protection [1,2]. The past two decades have witnessed the blossom of a variety of high-performance thermoelectric materials [3–7] along with new theories and design strategies. In recent years, thermoelectric technology has widely expanded its realm and found new applications in several booming industries, especially the self-powered flexible and nano/micro-scale electronics used as physiological monitors and wearable intelligent sensors [8,9]. To meet these conditions,

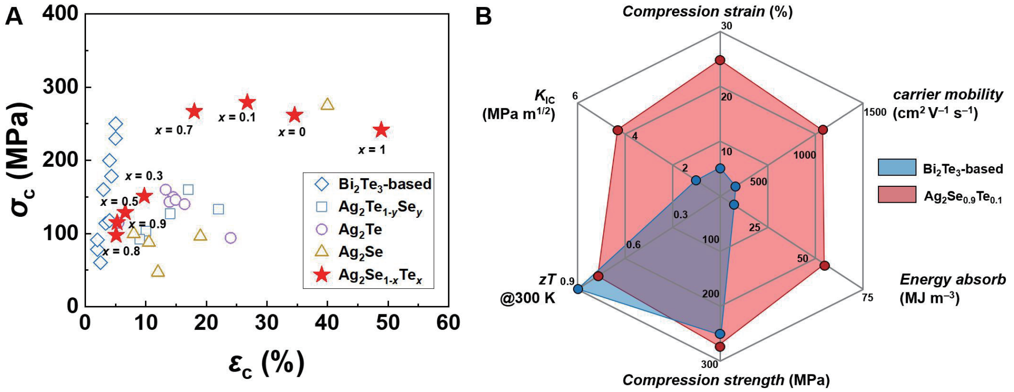

Figure 1 (A) Average values of the compression strength and ultimate strain for $Ag_2Se_{1-x}Te_x$ samples in this work (red stars); data of Ag_2Se [27,28,33], Ag_2Te [23,26], $Ag_2Te_{1-y}Se_y$ [26] and Bi_2Te_3-based polycrystalline thermoelectric materials [6,12–14,17–19] are included for comparison. Raw data are listed in Table S1. (B) Comparison of mechanical and physical properties between $Ag_2Se_{0.9}Te_{0.1}$ and typical Bi_2Te_3-based polycrystalline thermoelectric materials [6,12].

thermoelectric materials are required to possess both a high zT (defined as $zT = S^2\sigma T/\kappa$, where S, σ, T, and κ represent the Seebeck coefficient, electrical conductivity, absolute temperature, and thermal conductivity, respectively) and robust mechanical properties around room temperature to ensure decent processibility and deformability [10,11].

Traditional high-performance thermoelectric materials are typically brittle. For example, Bi_2Te_3-based polycrystalline alloys, the best room-temperature thermoelectric materials, show a small compressibility of merely ~5% [6,12–19] (Figure 1). As a consequence, seeking mechanically robust thermoelectric materials is a long-standing goal for promoting the application of thermoelectric devices. Fortunately, among the promising room-temperature thermoelectric materials, the Ag_2Se and Ag_2Te compounds are reported to show decent mechanical properties [20–28]: the compression strength and ultimate strain values can reach approximately 275 and 160 MPa, 40% and 20% for high-quality Ag_2Se and Ag_2Te samples, respectively. Interestingly, a large elongation of around 43% was found in nano-sized Ag_2Te material [26]. The introduction of domains and secondary phases was also employed to enhance the mechanical properties [23,27,28]. In addition to the pristine compounds, alloying is a classic and effective method to modulate transport and mechanical properties [29]. Feng *et al*. [26] studied the mechanical properties of Te-rich Ag_2(Te, Se) alloys, i.e., $Ag_2Te_{0.92}Se_{0.08}$, $Ag_2Te_{0.88}Se_{0.12}$, and $Ag_2Te_{0.8}Se_{0.2}$. The compression strains range from 10% to 22% and the strengths are 92–160 MPa.

Despite the above progress, the understanding of the mechanical properties of Ag_2(Se, Te) is still quite inadequate in terms of several aspects. Firstly, several key mechanical properties, such as fracture toughness and energy absorption, are overlooked in previous studies while these parameters are particularly important to evaluate materials ability to resist crack propagation. Secondly, for the Ag_2Se-Ag_2Te alloys, the mechanical study focuses only on Te-rich compositions (from Ag_2Te to $Ag_2Te_{0.8}Se_{0.2}$) [26] while a wide range of compositions remain to be explored. In addition, the underlying deformation mechanisms for this system need further exploration.

In this study, we comprehensively investigate the mechanical properties of Ag_2Se-Ag_2Te series materials, in terms of a wide range of compositions and diverse mechanical behaviors. It is found that this series of high-performance thermoelectric materials combines decent compressibility, strength, and toughness. As a case study, the high-performance $Ag_2Se_{0.9}Te_{0.1}$ material shows superior mechanical properties. Particularly, the fracture toughness of (4.5 ± 0.6) MPa $m^{1/2}$ is larger than typical thermoelectric counterparts like $(Bi, Sb)_2Te_3$, MgAgSb and $Mg_3(Sb, Bi)$-based materials [6,30,31]. Detailed microstructural analyses reveal that the large compressibility and toughness should originate from the dislocation multinucleation as well as the sub-grain rotation. This work demonstrates $Ag_2Se_{1-x}Te_x$ materials as promising thermoelectric materials with high performance and toughness for durable and stable thermoelectric devices.

MATERIALS AND METHODS

A series of $Ag_2Se_{1-x}Te_x$ samples were synthesized by a melting and annealing process followed by spark plasma sintering (SPS). High-purity elements Ag (shots, 99.99%, Alfa Aesar), Se (shots, 99.999%, Aladdin), and Te (shots, 99.999%, Aladdin) were weighted and then sealed in quartz tubes under vacuum. Slight Ag deficiencies were introduced in this procedure to finely tune the transport properties. The quartz tubes were slowly heated to 1273 K and kept at this temperature for 12 h. Afterwards, the tubes were cooled down to 1023 K over 25 h, and then to 723 K. After being dwelled at 723 K for 72 h, the tubes are naturally cooled down to room temperature. The as-prepared ingots were ground into powders under liquid nitrogen and dried in the oven at 338 K for 24 h to remove moisture. Powders were then consolidated by SPS at 623 K under the pressure of 55 MPa for 10 min.

The X-ray diffraction (XRD) was carried out with the Cu-Kα source with a scanning speed of 4°/min. The sample morphologies were examined by field emission scanning electron microscopy (FESEM, TESCAN RISE-MAGNA), along with energy dispersive X-ray analysis to observe elemental distribution. The transmission electron microscope (TEM) was characterized by FEI Talos F200X. The electrical conductivity and Seebeck coefficient were measured using ZEM-3 (Advanced Riko, Japan). The thermal conductivity was obtained via $\kappa = \lambda \times C_p \times d$, where λ is thermal diffusivity measured by Netzsch LFA-457, C_p is the heat capacity estimated by the Dulong-Petit law, and the density d was measured using Archimedes method. The differential scanning calorimetry was conducted on Netzsch DSC 404. The carrier concentration was measured by Lakeshore 8400 series using the van der Pauw method. The confocal laser scanning microscope test for the surface was performed on ZEISS LSM 900. Compression, three-point bending and fracture toughness tests were performed on SHIMADZU AGS-X. The specimen size is about 3 mm × 3 mm × 6.5 mm for compression with a constant strain rate of 0.005 min^{-1}, 2 mm × 1 mm × 18 mm for three-point bending and 3 mm × 2 mm × 18 mm with pre-crack length of 1.1 mm for fracture toughness. The loading speed for three-point bending and fracture toughness tests was set at 0.1 mm/min. The sound velocity data were measured by the ultrasonic measurement system UMS-100 with transverse wave transducers of 5 MHz and longitudinal wave transducers of 10 MHz.

RESULTS

Phase structures

For the $Ag_2Se_{1-x}Te_x$ samples, the XRD patterns (Figure S1) are indexed to the Ag_2Se-based orthorhombic

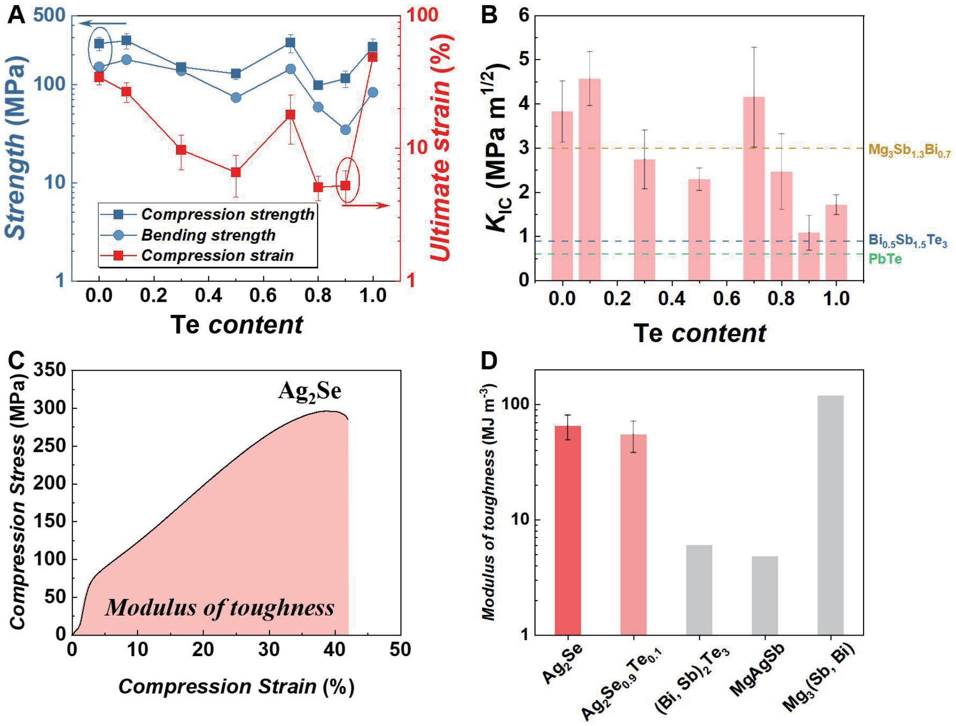

Figure 2 (A) Compression strength, compression strain and bending strength for $Ag_2Se_{1-x}Te_x$ samples. (B) Fracture toughness K_{IC} for $Ag_2Se_{1-x}Te_x$ samples; data of $Bi_{0.5}Sb_{1.5}Te_3$ [6], $Mg_3Sb_{1.3}Bi_{0.7}$ [31], PbTe [34] are also given for comparison. (C) Schematic illustration of energy absorption (modulus of toughness) for Ag_2Se under compression test. (D) Modulus of toughness for Ag_2Se, $Ag_2Se_{0.9}Te_{0.1}$ and other typical thermoelectric materials [12,30,35]. The error bars in panels A, B, and D denote the standard deviation from multiple measurements.

structure and Ag_2Te-based monoclinic structure when $x < 0.7$ and $x > 0.7$, respectively. For the composition of $x = 0.7$, the diffraction peaks are mainly indexed to Ag_2Se structure but a minor Ag_2Te-structured phase is also observed, indicating a mixed phase (also see Figure S2 for XRD refinement). The peaks shift to lower angles with increasing Te content in the Ag_2Se-structure region, which validates the alloying effect of Te in enlarging the lattice. All the Ag, Se, and Te elements show a homogeneous distribution as shown in Figure S1. With increasing Te content, the orthorhombic-to-cubic transition temperature slightly varies between 407 and 410 K as reflected by the DSC analysis (Figure S1). For the $Ag_2Se_{0.3}Te_{0.7}$ mixed-phase sample, two distinct endothermic peaks appear. This phase transition composition is also consistent with previous reports [32].

Mechanical properties

The compression stress-strain curves of $Ag_2Se_{1-x}Te_x$ samples are shown in Figure S3. Although there is a certain degree of data scattering, the average values are still useful for comparison. For both Ag_2Se and Ag_2Te, the average compression strength and strain well exceed 200 MPa and 30%, among the highest reported data for the two materials [23,33]. Compared with the pristine binary compounds, both the strength and compressibility decrease for the alloys, except two compositions: $Ag_2Se_{0.9}Te_{0.1}$ and $Ag_2Se_{0.3}Te_{0.7}$ (Figures 1A and 2A). As summarized in Figure 1A, the $Ag_2Se_{1-x}Te_x$ alloys are obviously more compressible and stronger than Bi_2Te_3-based materials (see raw data in Table S1). Taking $Ag_2Se_{0.9}Te_{0.1}$ as a typical case, the average compression strength is as high as 279.2 MPa and the average strain is 26.7%. For a couple of samples, the largest strength and strain can even reach around 300 MPa and 29%, respectively (Figure S3). The three-point bending test results are shown in Figure S3(i). The composition-dependent bending strength of the alloys is consistent with the compression strength. The Ag_2Se sample exhibits the maximum fractured bending strain of around 3% while other compositions show the values around 1%, a sign of brittle behavior in bending. The difference between bending and compression behaviors is well expected considering the different stress states.

The fracture toughness K_{IC}, the ability to resist the propagation of the crack, is also measured on single-edge notch-bending specimens (see the calculation detail in Supplementary Data). As shown in Figure 2B, the K_{IC} values share the similar tendency with the strength. The highest value of (4.5 ± 0.6) MPa $m^{1/2}$ appears at the composition $Ag_2Se_{0.9}Te_{0.1}$, which is higher than other thermoelectric materials like BiSbTe (0.9 MPa $m^{1/2}$) [6], PbTe (0.59 MPa $m^{1/2}$) [34], and $Mg_3Sb_{1.3}Bi_{0.7}$ (3.0 MPa $m^{1/2}$) [31]. Moreover, the integral of the area under stress-strain curves is often used to represent the total energy absorbed per unit volume up to failure as shown in Figure 2C. This value is termed as modulus of toughness, giving the overall measure of materials' ability to withstand both elastic and plastic deformation [35]. This parameter is especially important when facing a significant amount of impact. As shown in Figure 2D, this value is derived as (65 ± 16) MJ m^{-3} for Ag_2Se and (55 ± 17) MJ m^{-3} for $Ag_2Se_{0.9}Te_{0.1}$ from the compression stress-strain curve, much larger than most traditional thermoelectric materials. The high K_{IC} and modulus of toughness clearly indicate the tough and robust character of the materials.

Figure S5 shows the composition-dependent bulk modulus (B) and shear modulus (G) that are obtained from the measured sound speed. The bulk modulus is around 64 GPa for Ag_2Se and 48 GPa for Ag_2Te, which are comparable with the clathrate $Ba_8Ga_{16}Ge_{30}$ (66 GPa) and Mg_3Sb_2-based materials (45 GPa), and larger than hot-deformed Bi_2Te_3-based materials (ranging from 29 to 39 GPa) [6,36,37]. The alloyed samples show a slight decrease in modulus, which is consistent with the compression strength in Figure 2A.

Microstructural analysis

We perform detailed microstructural analyses to understand the origin of these robust mechanical properties. As shown in Figures S6 and S7, clear slip bands appear after compression for typical compositions $Ag_2Se_{0.9}Te_{0.1}$, Ag_2Se and Ag_2Te. In contrast, the bent samples exhibit intergranular fracture morphologies (Figure S4), suggesting the brittle behavior. Obvious dislocation lines are observed in broad regions in compressed $Ag_2Se_{0.9}Te_{0.1}$ (TEM bright-field image, Figure 3A and Figure S8) and some are further identified as dislocation arrays in a single grain (HRTEM, Figure 3B). The formation of dislocation arrays indicates the multiplication, movements and accumulation of dislocations in Ag_2(Se, Te) materials. The dislocation density estimated via the bright-field images is around 0.9×10^{14}–2.1×10^{14} m^{-2} (Figure S8), which is a high density comparable with 10% tensile deformed Cu metal [38]. The dual effects of dislocations on mechanical properties of these materials can be understood from two aspects. On the one hand, the existence, motion, and multiplication of dislocations can well mediate the compressive deformation by sliding and multiplication, which changes the large local stress into a long-range diffuse stress field and prevents stress concentration [39]. On the other hand, these high-density dislocations accompanied with large lattice strains can also further impair the plasticity and enhance the strength by entangling with each other just like in metals [40].

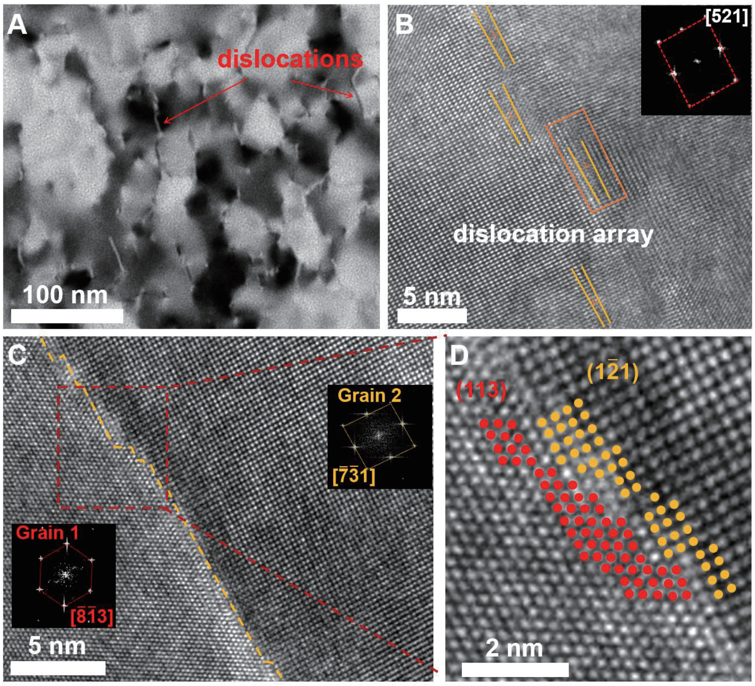

Figure 3 Transmission electron microscope (TEM) analysis of $Ag_2Se_{0.9}Te_{0.1}$ sample with a compression strain 10%. (A) Bright-field image showing typical dislocations marked by red arrows. (B) HRTEM image and corresponding FFT image highlighting the dislocation array. (C) HRTEM image illustrating two sub-grains; inset images are FFT images. (D) Grain interface of the red area in Panel (C); two sets of planes are marked as red and yellow dots, respectively.

Besides dislocations (Figure 3A and B), other mechanisms also contribute to the large compressibility and toughness. As shown in Figure 3C and D, a straight and coherent boundary is observed between Grain 1 and Grain 2 of the compressed $Ag_2Se_{0.9}Te_{0.1}$. The zone axes are [$\bar{8}\bar{1}3$] and [$\bar{7}\bar{3}1$], respectively and the corresponding planes at the boundary are (113) and ($1\bar{2}1$), respectively (Figure 3D). It is speculated that when undergoing compressive stress, the partial region of one grain is rotated against the other part, thus forming sub-grains with straight, coherent boundaries with certain orientation differences. More HRTEM images with similar structures are given in Figure S9. Compared with randomly oriented boundaries, the formation of these coherent or semi-coherent boundaries can effectively reduce internal stress and favor the plastic deformation rather than fracture in compression. Similar grain boundaries are also observed in compressed Ag_2Te as shown in Figure S10.

Thermoelectric transport properties

The temperature-dependent thermoelectric properties are shown in Figure S11. The transport properties of silver chalcogenides are sensitive to the Ag/anion ratio and fabrication methods [41,42]. In this study, we tuned the stoichiometry through introducing Ag deficiencies to obtain the optimal performance (Figure S12). To be concise, the compositions are still denoted as their stoichiometric ones. The Ag_2Se and $Ag_2Se_{0.9}Te_{0.1}$ samples exhibit high power factor PF of around 25 μW cm^{-1} K^{-2} compared with other compositions. According to the $|S|$-n_H plot (Pisarenko relation) shown in Figure 4A [43], the Ag_2Se-structure compositions have a relatively small density-of-state effective mass $m_d^* = 0.23m_e$ as compared with other typical ther-

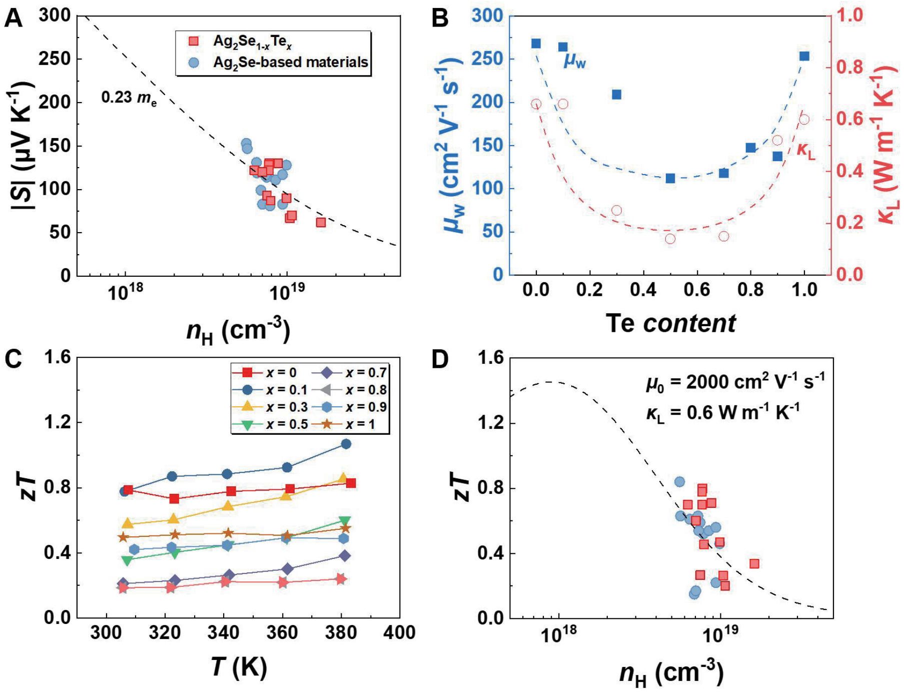

Figure 4 (A) Absolute Seebeck coefficient $|S|$ *versus* carrier concentration n_H for $Ag_2Se_{1-x}Te_x$ materials at 300 K. Data of other Ag_2Se-based materials are taken from Refs. [29,43]. The dashed line represents the calculated Pisarenko curve by the SPB model. (B) Relations of weighted mobility and lattice thermal conductivity with Te content; the dashed lines are calculated curves. (C) Temperature dependence of zT value for $Ag_2Se_{1-x}Te_x$ samples with optimized Ag content. (D) zT value *versus* carrier concentration n_H for $Ag_2Se_{1-x}Te_x$ materials at 300 K. Data of other Ag_2Se-based materials are taken from Refs. [29,43]. The dashed line represents the calculated Pisarenko curve by the SPB model.

moelectric materials (e.g., $1.12m_e$ for $Bi_2Te_{2.7}Se_{0.3}$ [44], $1.45m_e$ for GeTe [45], $2.3m_e$ for Cu_2Se [3]). The small effective mass is beneficial for electrical transport properties, especially the mobility. As shown in Figure 4B, the room-temperature weighted mobility μ_W, an integrated electrical performance indicator, readily decreases for the alloys, being a sign of alloy scattering of electrons.

As to the lattice thermal conductivity κ_L, the electrical conductivity is so high that the calculation based on the Wiedemann-Franz law and SPB-derived Lorenz number often suffers from large uncertainties. Instead, we employ a κ *versus* σ linear plot to derive κ_L as the intercept, which was proposed in our previous study [46] and illustrated in Figure S13. The κ_L firstly decreases from 0.66 W m^{-1} K^{-1} for Ag_2Se and $Ag_2Se_{0.9}Te_{0.1}$ to the minimum of 0.14 W m^{-1} K^{-1} for $Ag_2Se_{0.5}Te_{0.5}$, and then increases to 0.6 W m^{-1} K^{-1} for Ag_2Te, exhibiting a typical alloying effect trend [47] in which the mass and strain fluctuations can effectively scatter phonons. The variation of μ_w and κ_L with composition at room temperature is roughly fitted according to Ref. [48], which follows the relation of $\frac{1}{x(1-x)}$. It is worth mentioning that the varying trend of μ_w and κ_L with the composition is also consistent with that of the modulus (Figure S5). This means that apart from the alloy scattering effect, the lattice softening by alloying is also at play.

Figure 4C shows the temperature-dependent zT for a series of $Ag_2Se_{1-x}Te_x$ materials. Combining decent *PF*s and low thermal conductivity, the $Ag_2Se_{0.9}Te_{0.1}$ material shows a high zT value of 0.78 at room temperature and 1.1 at 380 K. Using the single parabolic model [49], assuming the non-degenerate limit of mobility, μ_0, as 2000 cm^2 V^{-1} s^{-1} and lattice thermal conductivity as 0.6 W m^{-1} K^{-1}, the theoretical curve of *zT versus* n_H is plotted in Figure 4D. If the carrier concentration can be further optimized to 1×10^{18}–2×10^{18} cm^{-3}, the room-temperature zT will be further enhanced to above unity.

DISCUSSION

In this work, the phase structures, mechanical and thermoelectric properties of $Ag_2Se_{1-x}Te_x$ alloys are studied. Te alloying transforms the orthorhombic Ag_2Se into the monoclinic phase at the composition of x~0.7. The orthorhombic Ag_2Se-rich materials exhibit higher thermoelectric performance, especially for the $Ag_2Se_{0.9}Te_{0.1}$ sample. The zT value can reach 0.78 at room temperature and 1.1 at 380 K. Noticeably, $Ag_2Se_{0.9}Te_{0.1}$ exhibits superior mechanical robustness with high strength of (279.2 ± 49) MPa, decent compressibility of (26.7 ± 4.5)%, and large fracture toughness of (4.5 ± 0.6) MPa $m^{1/2}$. The robust mechanical properties are attributed to the dense dislocations and possible sub-grain rotations. These findings will advance the understanding of the mechanical properties of Ag_2Se/Ag_2Te-based alloys and help develop robust and efficient thermoelectric materials around room temperature.

Data availability

The original data are available from corresponding authors upon reasonable request.

Funding

Tian-Ran Wei was supported by the National Natural Science Foundation of China (92463310, 52373292). Tian-Ran Wei and Kunpeng Zhao were supported by the Zhejiang Provincial Natural Science Foundation of China (LD25E020001). Xun Shi was supported by the National Natural Science Foundation of China (52232010).

Author contributions

T.-R.W. and X.S. designed the research. H.C., S.R., and H.F. did the experiment. L.F. and Z.P. helped conduct the mechanical property test. H.C. wrote the manuscript. T.-R.W., Z.P., K.Z., X.L., and X.S. revised the manuscript.

Conflict of interest

The authors declare no conflict of interest.

Supplementary information

The supporting information is available online at https://doi.org/10.1360/20250005. The supporting materials are published as submitted, without typesetting or editing. The responsibility for scientific accuracy and content remains entirely with the authors.

References

1 He J, Tritt TM. Advances in thermoelectric materials research: Looking back and moving forward. *Science* 2017; **357**: eaak9997.

2 Zhu T, Liu Y, Fu C, *et al.* Compromise and synergy in high-efficiency thermoelectric materials. *Adv Mater* 2017; **29**: 1605884.

3 Liu H, Shi X, Xu F, *et al.* Copper ion liquid-like thermoelectrics. *Nat Mater* 2012; **11**: 422–425.

4 Zhang Z, Zhao K, Chen H, *et al.* Entropy engineering induced exceptional thermoelectric and mechanical performances in $Cu_{2-y}Ag_yTe_{1-2x}S_xSe_x$. *Acta Mater* 2022; **224**: 117512.

5 Poudel B, Hao Q, Ma Y, *et al.* High-thermoelectric performance of nanostructured bismuth antimony telluride bulk alloys. *Science* 2008; **320**: 634–638.

6 Zheng Y, Zhang Q, Su X, *et al.* Mechanically robust BiSbTe alloys with superior thermoelectric performance: A case study of stable hierarchical nanostructured thermoelectric materials. *Adv Energy Mater* 2015; **5**: 1401391.

7 Mao J, Zhu H, Ding Z, *et al.* High thermoelectric cooling performance of n-type Mg_3Bi_2-based materials. *Science* 2019; **365**: 495–498.

8 Zhao X, Yang S, Wen X, *et al.* A fully flexible intelligent thermal touch panel based on intrinsically plastic Ag_2S semiconductor. *Adv Mater* 2022; **34**: 2107479.

9 Yang Q, Yang S, Qiu P, *et al.* Flexible thermoelectrics based on ductile semiconductors. *Science* 2022; **377**: 854–858.

10 Wei T, Qiu P, Zhao K, *et al.* Ag_2Q-Based (Q = S, Se, Te) silver chalcogenide thermoelectric materials. *Adv Mater* 2023; **35**: 2110236.

11 Ma Y, Huang H, Liu Y, *et al.* Remarkable plasticity and softness of polymorphic InSe van der Waals crystals. *J Materiomics* 2023; **9**: 709–716.

12 Qin H, Qu W, Zhang Y, *et al.* Nanotwins strengthening high thermoelectric performance bismuth antimony telluride alloys. *Adv Sci* 2022; **9**: 2200432.

13 Zhu Y, Sun Y, Zhu J, *et al.* Mediating point defects endows n-Type Bi_2Te_3 with high thermoelectric performance and superior mechanical robustness for power generation application. *Small* 2022; **18**: 2201352.

14 Wang W, Sun Y, Feng Y, *et al.* High thermoelectric performance bismuth telluride prepared by cold pressing and annealing facilitating large scale application. *Mater Today Phys* 2021; **21**: 100522.

15 Chen H, Wei T, Zhao K, *et al.* Room-temperature plastic inorganic semiconductors for flexible and deformable electronics. *InfoMat* 2021; **3**: 22–35.

16 Qiu J, Yan Y, Luo T, *et al.* 3D Printing of highly textured bulk thermoelectric materials: Mechanically robust BiSbTe alloys with superior performance. *Energy Environ Sci* 2019; **12**: 3106–3117.

17 Qiu J, Yan Y, Xie H, *et al.* Achieving superior performance in thermoelectric $Bi_{0.4}Sb_{1.6}Te_{3.72}$ by enhancing texture and inducing high-density line defects. *Sci China Mater* 2021; **64**: 1507–1520.

18 Sun Y, Guo F, Feng Y, *et al.* Performance boost for bismuth telluride thermoelectric generator via barrier layer based on low Young’s modulus and particle sliding. *Nat Commun* 2023; **14**: 8085.

19 Zhu Y, Jin Y, Zhu J, *et al.* Design of n-type textured Bi_2Te_3 with robust mechanical properties for thermoelectric micro-refrigeration application. *Adv Sci* 2023; **10**: 2206395.

20 Ferhat M, Nagao J. Thermoelectric and transport properties of β-Ag_2Se compounds. *J Appl Phys* 2000; **88**: 813–816.

21 Mi W, Qiu P, Zhang T, *et al.* Thermoelectric transport of Se-rich Ag_2Se in normal phases and phase transitions. *Appl Phys Lett* 2014; **104**: 133903.

22 Huang S, Wei TR, Chen H, *et al.* Thermoelectric Ag_2Se: Imperfection, homogeneity, and reproducibility. *ACS Appl Mater Interfaces* 2021; **13**: 60192–60199.

23 Wang H, Feng X, Lu Z, *et al.* Synergetic enhancement of strength-ductility and thermoelectric properties of Ag_2Te by domain boundaries. *Adv Mater* 2023; **35**: 2302969.

24 Peng L, Yang S, Wei TR, *et al.* Phase-modulated mechanical and thermoelectric properties of $Ag_2S_{1-x}Te_x$ ductile semiconductors. *J Materiomics* 2022; **8**: 656–661.

25 Huang H, Chen H, Gao Z, *et al.* Room-temperature wide-gap inorganic materials with excellent plasticity. *Adv Funct Mater* 2023; **33**: 2306042.

26 Feng L, Guo A, Liu K, *et al.* Highly deformable $Ag_2Te_{1-x}Se_x$-based thermoelectric compounds. *Mater Today Phys* 2023; **33**: 101051.

27 Chen J, Sun Q, Bao D, *et al.* Simultaneously enhanced strength and plasticity of Ag_2Se-based thermoelectric materials endowed by nano-twinned CuAgSe secondary phase. *Acta Mater* 2021; **220**: 117335.

28 Wang H, Liu X, Zhou Z, *et al.* Constructing n-type Ag_2Se/CNTs composites toward synergistically enhanced thermoelectric and mechanical performance. *Acta Mater* 2022; **223**: 117502.

29 Liang J, Qiu P, Zhu Y, *et al*. Crystalline structure-dependent mechanical and thermoelectric performance in $Ag_2Se_{1-x}S_x$ system. *Research* 2020; **2020**: 6591981.

30 Liu Z, Gao W, Meng X, *et al.* Mechanical properties of nanostructured thermoelectric materials α-MgAgSb. *Scripta Mater* 2017; **127**: 72–75.

31 Shu R, Zhou Y, Wang Q, *et al.* $Mg_{3+\delta}Sb_xBi_{2-x}$ family: A promising substitute for the state-of-the-art n-type thermoelectric materials near room temperature. *Adv Funct Mater* 2019; **29**: 1807235.

32 Zhu T, Su X, Zhang Q, *et al.* Structural transformation and thermoelectric performance in $Ag_2Te_{1-x}Se_x$ solid solution. *J Alloys Compd* 2021; **871**: 159507.

33 Liu M, Zhang X, Zhang S, *et al.* Ag_2Se as a tougher alternative to n-type Bi_2Te_3 thermoelectrics. *Nat Commun* 2024; **15**: 6580.

34 Li G, Aydemir U, Duan B, *et al.* Micro- and macromechanical properties of thermoelectric lead chalcogenides. *ACS Appl Mater Interfaces* 2017; **9**: 40488–40496.

35 Li A, Wang Y, Li Y, *et al.* High performance magnesium-based plastic semiconductors for flexible thermoelectrics. *Nat Commun* 2024; **15**: 5108.

36 Isotta E, Peng W, Balodhi A, *et al.* Elastic moduli: A tool for understanding chemical bonding and thermal transport in thermoelectric materials. *Angew Chem Int Ed* 2023; **62**: e202213649.

37 Agne M T, Imasato K, Anand S, *et al.* Heat capacity of Mg_3Sb_2, Mg_3Bi_2, and their alloys at high temperature. *Mater Today Phys* 2018; **6**: 83–88.

38 Jiang J, Britton TB, Wilkinson A J. Evolution of dislocation density distributions in copper during tensile deformation. *Acta Mater* 2013; **61**: 7227–7239.

39 Bacon DJ, Hull D. *Introduction to Dislocations*. Amsterdam: Elsevier, 2011.

40 Zhang BB, Yan FK, Zhao MJ, *et al.* Combined strengthening from nanotwins and nanoprecipitates in an iron-based superalloy. *Acta Mater* 2018; **151**: 310–320.

41 Li D, Zhang JH, Li JM, *et al.* High thermoelectric performance for an Ag_2Se-based material prepared by a wet chemical method. *Mater Chem Front* 2020; **4**: 875–880.

42 Yang D, Su X, Meng F, *et al.* Facile room temperature solventless synthesis of high thermoelectric performance Ag_2 Se *via* a dissociative adsorption reaction. *J Mater Chem A* 2017; **5**: 23243–23251.

43 Liang J, Liu J, Qiu P, *et al.* Modulation of the morphotropic phase boundary for high-performance ductile thermoelectric materials. *Nat Commun* 2023; **14**: 8442.

44 Liu W, Zhang Q, Lan Y, *et al.* Thermoelectric property studies on Cu-doped n-type $Cu_xBi_2Te_{2.7}Se_{0.3}$ nanocomposites. *Adv Energy Mater* 2011; **1**: 577–587.

45 Hong M, Wang Y, Liu W, *et al.* Arrays of planar vacancies in superior thermoelectric $Ge_{1-x-y}Cd_xBi_yTe$ with band convergence. *Adv Energy Mater* 2018; **8**: 1801837.

46 Chen H, Shao C, Huang S, *et al.* High-entropy cubic pseudo-ternary Ag_2(S, Se, Te) materials with excellent ductility and thermoelectric performance. *Adv Energy Mater* 2024; **14**: 2303473.

47 Wang H, Pei Y, LaLonde AD, *et al.* Weak electron-phonon coupling contributing to high thermoelectric performance in n-type PbSe. *Proc Natl Acad Sci USA* 2012; **109**: 9705–9709.

48 Wei TR, Tan G, Wu CF, *et al.* Thermoelectric transport properties of polycrystalline SnSe alloyed with PbSe. *Appl Phys Lett* 2017; **110**: 053901.

49 Yang S, Gao Z, Qiu P, *et al.* Ductile $Ag_{20}S_7Te_3$ with excellent shape-conformability and high thermoelectric performance. *Adv Mater* 2021; **33**: 2007681.